Catal Lett (2009) 128:83–93
DOI 10.1007/s10562-008-9737-5

# Physicochemical Characterization of $Al_2O_3$ Supported Ni–Rh Systems and their Catalytic Performance in $CH_4/CO_2$ Reforming

**M. Nowosielska · W. K. Jozwiak · J. Rynkowski**

Received: 28 July 2008 / Accepted: 15 October 2008 / Published online: 13 November 2008


**Abstract** Activity and stability of alumina-supported monometallic Ni, Rh and bimetallic Ni–Rh catalysts were studied towards carbon dioxide reforming of methane. The catalysts were prepared by the incipient wetness impregnation method with different contents of Rh and Ni and were characterized by $H_2$ chemisorption, $TPR_{H2}$, XRD, FT-IR and ToF-SIMS methods. The process of Ni–Rh alloy formation and nickel enrichment on alloy surface takes place during temperature-programmed hydrogen assisted decomposition of their precursors. Catalytic stability and resistance towards coke deposition for $Rh/Al_2O_3$ and $Ni–Rh/Al_2O_3$ catalysts are much higher than for $Ni/Al_2O_3$ and $Ni–Rh/SiO_2$ systems, studied in the first part of this paper (Jóźwiak WK, Nowosielska M, Rynkowski JM, Appl. Catal. A 280:233, 2005).

**Keywords** $CO_2$ reforming of methane · Ni–Rh · $Al_2O_3$ · TP techniques · XRD · FTIR · ToF-SIMS · TOC

## 1 Introduction

In the previous paper [1], the influence of active phase composition on reducibility of silica-supported monometallic Ni, Rh and bimetallic Ni–Rh catalysts and their activity in reaction of carbon dioxide reforming of methane were investigated. It was found that the effective process of Ni–Rh alloy formation takes place on silica surface but only Rh-rich systems appeared highly resistant to deactivation and coke formation. The different behavior of Ni-rich bimetallic catalysts was related to a different degree of metal–metal interaction and enrichment of metallic alloy surface in nickel.

In the present paper physicochemical and catalytic properties of alumina supported monometallic Ni, Rh and bimetallic Ni–Rh catalysts were studied towards carbon dioxide reforming of methane. Wang and Ruckenstein [2] studied the effect of support on the performance of Rh-based catalysts in $CO_2$ reforming of methane. They stated that the most promising supports for this reaction are $Al_2O_3$ and MgO—irreducible oxides, which provide much higher yields to CO and $H_2$ than the reducible ones. Aluminum oxide was also found to be an effective support in this regard in other papers [3–5]. Therefore, an effort was made to study bimetallic $Ni–Rh/Al_2O_3$ catalysts. The catalysts were characterized by $H_2$ chemisorption, temperature-programmed reduction with hydrogen ($TPR_{H2}$), X-ray diffraction (XRD), Fourier transform infrared spectroscopy (FT-IR) and time of flight secondary ions mass spectrometry (ToF-SIMS) while the coke deposit was detected by the total carbon analysis (TOC).

## 2 Experimental

### 2.1 Catalyst Preparation

Support-$\gamma$-$Al_2O_3$ (Fluka AG 507C) with the surface area of 136 $m^2\ g^{-1}$ and pores with diameter about 2.3 nm was impregnated with aqueous solutions of $Ni(NO_3)_2$, $RhCl_3$ or $Rh(NO_3)_3$ by the incipient wetness method. The bimetallic $Ni–Rh/Al_2O_3$ catalysts were prepared by co-impregnated

The work was presented during the conference 'Catalysis for Society', Krakow, May 11–15, 2008.

M. Nowosielska (✉) · W. K. Jozwiak · J. Rynkowski
Institute of General and Ecological Chemistry,
Technical University of Lodz, ul. Zeromskiego 116,
90-924 Lodz, Poland
e-mail: mlefik@p.lodz.pl

method. The catalyst precursors were dried at 105 °C for 12 h, then calcined at 500 °C for 3 h in an oxygen flow and finally reduced in situ at 600 °C in flowing hydrogen stream before being tested. The average particle size of the catalyst grains was in the range 1–2.5 × $10^2$ μm. The catalyst denotation and nominal composition of the catalysts are presented in Table 1. The estimated experimental values of metal contents verified by ICP-ASA method were found in the range ±5% of the nominal values.

## 2.2 Catalyst Characterization

### 2.2.1 $H_2$ Chemisorption

Hydrogen chemisorption uptakes were measured by the static equilibrium $H_2$ chemisorption method at a temperature of 35 °C using ASAP 2010C apparatus from Micromeritics (USA). All catalysts were degassed and reduced in situ prior to hydrogen chemisorption. The catalyst surface purification procedure of ca. 1 g catalyst was performed in flowing helium at 500 °C for 1 h and reduction was carried out in flowing hydrogen at 600 °C for 1 h.

### 2.2.2 $TPR_{H2}$ and TPO

An AMI1 system from Altamira Instruments (USA) equipped with a thermal conductivity detector (TCD) was used for the $TPR_{H2}$ and TPO experiments. In these measurements mixtures of 5 vol.% $H_2$ and 95 vol.% Ar or 2 vol.% $O_2$ and 98 vol.% Ar, respectively, were used at space velocity $W/F = 1.11 \times 10^{-5}$ g h $cm^{-3}$ and a linear growth of temperature 20 °C $min^{-1}$. In order to study the temperature-programmed hydrogen assisted decomposition ($TPDec_{H2}$) of catalyst precursors, sintering processes and the influence of the calcination/reoxidation temperature on Ni–Rh/$Al_2O_3$ catalyst behaviors, following temperature-programmed experiments were carried out:

– some of the catalyst precursors were subjected to $TPDec_{H2}$, followed by successive TPO–$TPR_{H2}$ cycles:

TPO500 °C → $TPR_{H2}$900 °C → TPO700 °C → $TPR_{H2}$900 °C → TPO900 °C → $TPR_{H2}$900 °C;

– some of the catalysts were initially calcined in $O_2$/Ar atmosphere at temperatures 500, 700 and 900 °C, respectively. Oxidation was followed by $TPR_{H2}$ up to 900 °C.

$TPDec_{H2}$ of monometallic Rh and bimetallic Ni–Rh catalyst precursors prepared from $Rh(NO_3)_3$ was carried out in a conventional flow microreactor connected with a quadrupole mass spectrometer (MS-Dycor 1000) used as a detector.

### 2.2.3 XRD

XRD measurements were carried out in the Siemens D5000 polycrystalline diffractometer using $CuK_\alpha$ radiation (0.151418 nm). The scan rate was 0.03°/10 s for 2$\theta$ range 2°–80°.

### 2.2.4 FT-IR

FT-IR experiments were performed using a Shimadzu FT-IR spectrometer equipped with a transmission cell and liquid nitrogen-cooled MCT detector. The cell, containing cooled ZnSe windows, allowed in situ collection of spectra in the temperature range 25–800 °C at atmospheric pressure. For all spectra, 40 scan data acquisition was carried out at a resolution of 4.0 $cm^{-1}$. Samples were in the form of self-supporting wafers and weighed about 20 mg.

In a typical experiment the sample of catalyst previously calcined in $O_2$ at 500 °C for 3 h and reduced in $H_2$ at 600 °C for 1 h was heated in flowing $H_2$ up to 500 °C and was subsequently reduced in situ for 30 min. After cooling to room temperature in flowing Ar and collecting background spectrum, CO was admitted at atmospheric pressure

**Table 1** Chemical composition and results of hydrogen chemisorption measurements

| No. | Catalyst | Nominal metal content (wt.%) | | $H_2$ uptake ($cm^3_{(STP)}$ $g^{-1}_{cat}$) | Dispersion (%) | Metallic surface area ($m^2$ $g^{-1}_{cat}$) | Metallic surface area ($m^2$ $g^{-1}_{metal}$) | Crystallite size (nm) |
|---|---|---|---|---|---|---|---|---|
| | | Ni | Rh | | | | | |
| 1 | 5Ni | 5 | 0 | 0.22 | 2.3 | 0.77 | 15.4 | 43.7 |
| 2 | 3.75Ni–1.25Rh | 3.75 | 1.25 | 0.30 | 3.5 | 1.08 | 21.6 | 28.3 |
| 3 | 2.5Ni–2.5Rh | 2.5 | 2.5 | 0.29 | 3.8 | 1.07 | 21.4 | 26.3 |
| 4 | 1.25Ni–3.75Rh | 1.25 | 3.75 | 1.08 | 16.7 | 4.15 | 83.0 | 6.23 |
| 5 | 5Rh | 0 | 5 | 2.06 | 37.8 | 8.32 | 166.4 | 2.90 |
| 6 | 2.5Ni–2.5Rh(n) | 2.5 | 2.5 | 1.21 | 16.2 | 4.47 | 89.4 | 6.27 |
| 7 | 5Rh(n) | 0 | 5 | 2.16 | 39.7 | 8.73 | 174.6 | 2.75 |

(n) indicates precursor of Rh–$Rh(NO_3)_3$

for 15 min at 25 °C and FT-IR spectra were collected. After that CO desorption was performed by flushing with Ar.

#### 2.2.5 ToF-SIMS

The secondary ions mass spectra were recorded with a ToF-SIMS IV mass spectrometer manufactured by Ion-Tof GmbH, Muenster, Germany. The instrument is equipped with metal $Bi^+$ primary ion gun and high mass resolution time of flight mass analyzer. Secondary ion mass spectra were recorded from an approximately 500 μm × 500 μm area of the catalysts surface: 2.5Ni–2.5Rh/$Al_2O_3$ prepared from $RhCl_3$ precursor calcined at 500 °C/3 h in an oxygen flow and next after its reduction at 600 °C/1 h in hydrogen stream. The analysis time was 30 s giving an ion dose below static limit of $7.5 \times 10^{10}$ ions/cm$^2$. During measurement in the beginning the spectra for "as prepared" catalysts were collected and then the same area was subjected to surface sputtering using $Bi^+$ ions beam per 60 s (direct current—about 17 nA), which resulted in removal of some part of surface layers of the analyzed samples. Soon afterwards, next spectra were recorded from the same area.

### 2.3 Catalytic Test

The sample about 100 mg of catalyst was loaded into a tubular quartz microreactor and the temperature of catalyst bed was measured by a thermocouple. The catalysts were calcined in $O_2$ stream at 500 °C for 3 h and reduced in situ in $H_2$ at 600 °C for 1 h before the catalytic activity measurements. All activity tests were carried out under atmospheric pressure with equimolar stoichiometric mixture of $CH_4$ and $CO_2$ (50 vol.% of each gas) and a total feed flow rate of 50 cm$^3$ min$^{-1}$ (space velocity $W/F = 3.33 \times 10^{-5}$ g h cm$^{-3}$), in the temperature range 300–900 °C at intervals of 50 °C, keeping catalyst during 0.5 h at this temperature. The catalyst lifetime test was performed for 24 h at a temperature of 700 °C. The reaction products were analyzed using an *on-line* gas chromatograph (Varian 3300), equipped with a CTR1 column and a thermal conductivity detector (TCD). The activity was expressed as "turnover frequency number of CO" ($TOF_{CO}$) and as "$mol_{CO}\ g_{cat}^{-1}\ h^{-1}$".

### 2.4 Total Carbon (TC)

The total amount of carbon on the surface of used catalysts was determined by Shimadzu Total Carbon Analyser (TOC 5000) connected with Solid Sample Module (SSM–5000A).

## 3 Results and Discussion

### 3.1 Catalyst Characterization

The results of hydrogen chemisorption measurements, metal dispersion, metal surface area and average crystallite size for catalysts are presented in Table 1. Additionally, composition of Ni–Rh catalysts and their denotation are also included.

Metal dispersion $Me_s/Me$ was expressed as $H_c/Me$ ratio and calculated assuming chemisorption stoichiometric coefficient $H_c/Me_s = 1$ both for monometallic and bimetallic catalysts. The examination of these results shows a significantly lower dispersion degree of nickel (about 2%) than rhodium (38–40%) for the monometallic catalysts supported on alumina surface. Metal surface area and average crystallite size for the bimetallic catalysts were calculated on the following assumptions: every surface metal atom, whether it is nickel or rhodium, is chemically bonded with hydrogen with a stoichiometric coefficient $H/Me_s = 1$; full alloying of metal components and the resultant bulk and surface metal site densities [6] were calculated assuming the nominal composition of catalysts; metallic particle size was calculated assuming spherical shape and appropriate density of metals or alloy. Metal dispersion for bimetallic Ni–Rh catalysts is in the range embraced by those limits characteristic of nickel and rhodium dispersion degrees. Slightly higher dispersion of rhodium phase is observed for the catalyst obtained from nitrate precursor.

On the basis of hydrogen chemisorption measurements (Table 1) the plot of hydrogen uptake versus Ni–Rh bulk composition of supported catalysts is presented in Fig. 1.

The straight dashed line represents the expected theoretical values when a full miscibility of metallic components takes place on alumina support and the composition of bulk alloy and that characteristic of surface composition are identical. The experimental solid line shows a negative decline in relation to theoretical assumptions and these effects can be attributed to nickel enrichment on the surface of bimetallic Ni–Rh phase. On the basis of Williams and Nason paper [7] such a behavior of nickel can be expected for Ni–Rh alloy taking into account the thermodynamic values of sublimation enthalpy for nickel $\Delta H° = -430$ kJ/mol and for rhodium $\Delta H° = -553$ kJ/mol [8]. A much lower value of nickel sublimation enthalpy would facilitate nickel surface enrichment during high temperature hydrogen reduction of oxidized bimetallic Ni–Rh catalysts. Also, in the case of silica supported bimetallic Ni–Rh [1] system, the surface enrichment in Ni was shown. The formation of bulk Ni–Rh alloys seems to be confirmed by XRD

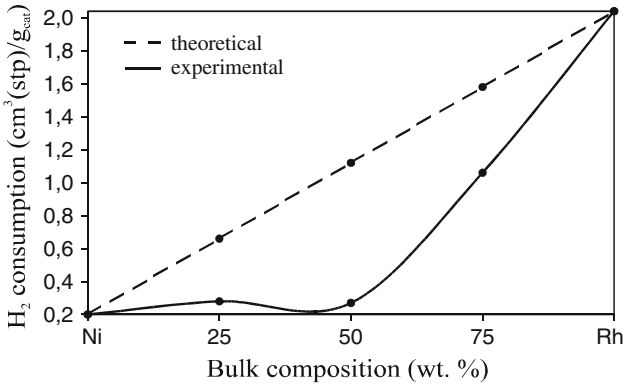


**Fig. 1** $H_2$ chemisorption on Ni–Rh/$Al_2O_3$ catalysts (at 35 °C) prepared from $Ni(NO_3)_2$ and $RhCl_3$ in function of metal phase bulk composition

measurements (see also Figs. 6, 7). In literature, one can find the examples of Ni surface enrichment in Ni–Rh alloy dispersed on alumina [9], the formation of surface Ni–Rh alloy on $La_2O_3$ surface [10] and on $ZrO_2$ surface [11].

The temperature-programmed hydrogen assisted decomposition profiles of Ni–Rh/$Al_2O_3$ catalyst precursors prepared from $Ni(NO_3)_2$, and two kinds of rhodium salts—$RhCl_3$ and $Rh(NO_3)_3$ are illustrated in Fig. 2a and b, respectively.

The supported $Ni(NO_3)_2$/alumina system after drying at an ambient temperature undergoes two step reduction stages [12] according to the following equations: the first peak with maximum at about 300 °C

$$Ni(NO_3)_2 + (5-2x)H_2 \rightarrow NiO + 2NO_x + (5-2x)H_2O \quad (x = 0, 0.5, 1, 1.5, \text{or } 2) \tag{1}$$

and the second one with maximum at about 495 °C

$$NiO + H_2 \rightarrow Ni + H_2O \tag{2}$$

Different nitrogen oxides $NO_x$ (x = 0, 0.5, 1, 1.5 or 2) can be detected by mass spectrometry, but nitrogen monoxide NO predominates as a primary product of the first step of decomposition, taking place according to Eq. 1. Nickel nitrate dispersed on alumina is transformed into nickel monoxide NiO. The second step of catalyst decomposition represents the reduction of NiO into metallic nickel on alumina surface and is illustrated by simple Eq. 2. A similar decomposition scheme was observed for analogous Ni/$SiO_2$ catalyst precursor [1].

The unsupported hydrated $Rh(NO_3)_3$ decomposes as a partly overlapped three step process: dehydration, rhodium nitrate and rhodium oxide reduction. Analogical behaviour can be expected on alumina surface but the high dispersion of active phase precursor shifts the $H_2$ reduction decomposition to an even lower temperature making it a highly overlapped three step process, which can be expressed by the following equations:

$$Rh(NO_3)_3 \cdot 6H_2O \rightarrow Rh(NO_3)_3 + 6H_2O \quad (T_{max.} \text{ at } 125\ ^\circ C) \tag{3}$$

$$2Rh(NO_3)_3 + 3(5-2x)H_2 \rightarrow Rh_2O_3 + 6NO_x + 3(5-2x)H_2O \quad (x = 0, 0.5, 1, 1.5 \text{ or } 2) \quad (T_{max.} \text{ at } 165\ ^\circ C) \tag{4}$$

$$Rh_2O_3 + 3H_2 \rightarrow 2Rh + 3H_2O \quad (T_{max.} \text{ at } 210\ ^\circ C) \tag{5}$$

The $RhCl_3$ phase supported on alumina can undergo two step reduction stages according to the following equations:

$$RhCl_3 + H_2 \rightarrow RhCl + 2HCl \quad (T_{max.} \text{ at } 65\ ^\circ C) \tag{6}$$

$$RhCl + 0.5H_2 \rightarrow Rh + HCl \quad (T_{max.} \text{ at } 150\ ^\circ C) \tag{7}$$

However, evolution of hydrogen chloride to gas phase was not observed probably because of the subsequent reaction of HCl species with surface hydroxyl groups of alumina taking place according to the following scheme:

$$HCl + OH^-_{(s)} \rightarrow H_2O + Cl^-_{(s)} \tag{8}$$

The significant amount of chlorine species adsorbed on alumina surface was detected after high-temperature catalyst calcinations at 800 °C in air by ToF-SIMS method [13]. The temperature range of reduction profiles for monometallic nickel and rhodium oxide phases are separated almost entirely, as it can be seen from curves 1, 5 and 7 in Fig. 2. The temperature range 50–400 °C is characteristic of the reduction of bimetallic Ni–Rh precursors occurring practically in one stage (curves 2–4 and 6 in Fig. 2). Such a course of reduction can be attributed to a mixed coordination sphere of nickel and rhodium ions surrounded by nitrate and chlorine ions. The same effects were observed for Ni–Rh/$SiO_2$ catalysts [1]. A very close vicinity of nickel and rhodium ions is anticipated and this direct contact seems to be the unavoidable prerequisite condition of Ni and Rh mixing during the alloy formation. Also, the presence of rhodium metal species promotes the reduction of nickel ions to the metal phase, preventing the intermediate formation of NiO phase, as it was in the case of monometallic nickel catalyst precursor reduction (curves 1 in Fig. 2a, b). Hou and Yashima [14] studied hydrogen temperature programmed reduction of Rh-promoted Ni/α-$Al_2O_3$ catalysts and concluded a strong interaction between Rh and Ni, which can retard the sintering of Ni phase.

The influence of calcination temperature of nitrate-based catalyst in oxygen stream, 1 h at 500, 700 and 900 °C on $TPR_{H2}$ profiles is illustrated in Fig. 3.

The general trend of a profile shift towards higher temperatures can be observed when the temperature of oxidation is increased from 500 to 700 °C and especially to 900 °C. In the case of 5Rh/$Al_2O_3$ catalyst the small crystallites of rhodium oxide not interacting with the support, with the average diameter of about 3 nm exist on alumina

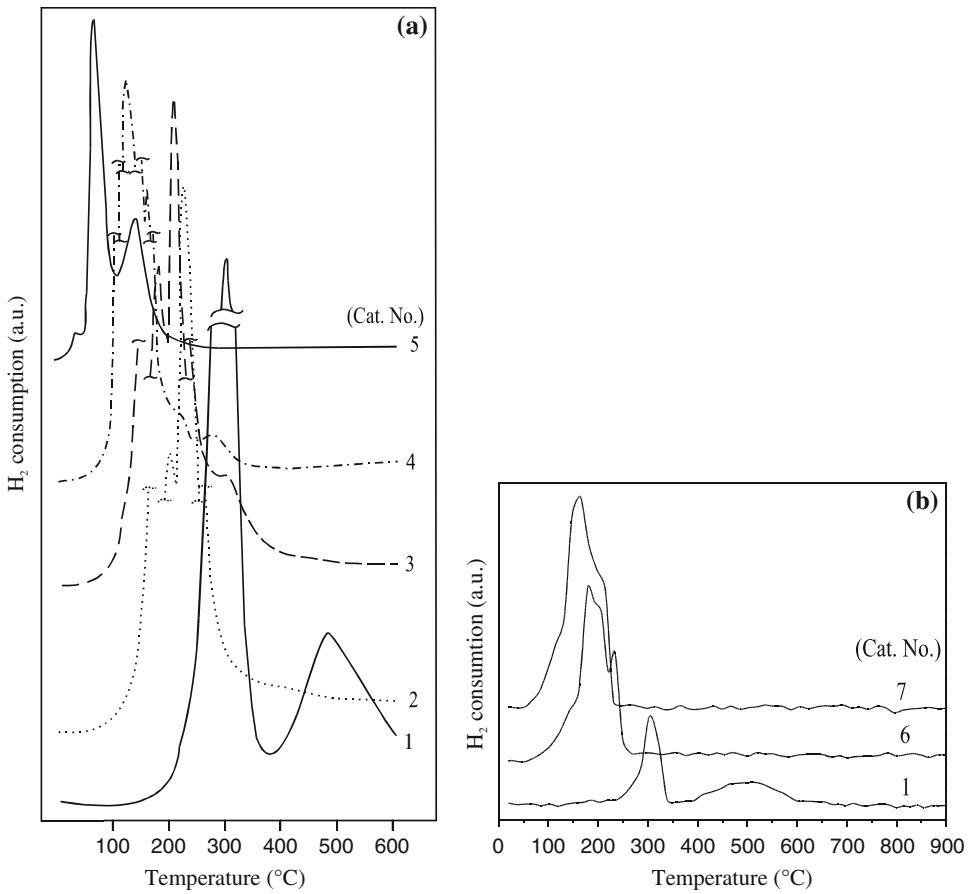


**Fig. 2** $TPDec_{H2}$ profiles of Ni–Rh/$Al_2O_3$ catalyst precursors prepared from **a** $Ni(NO_3)_2$, $RhCl_3$ and **b** $Ni(NO_3)_2$, $Rh(NO_3)_3$

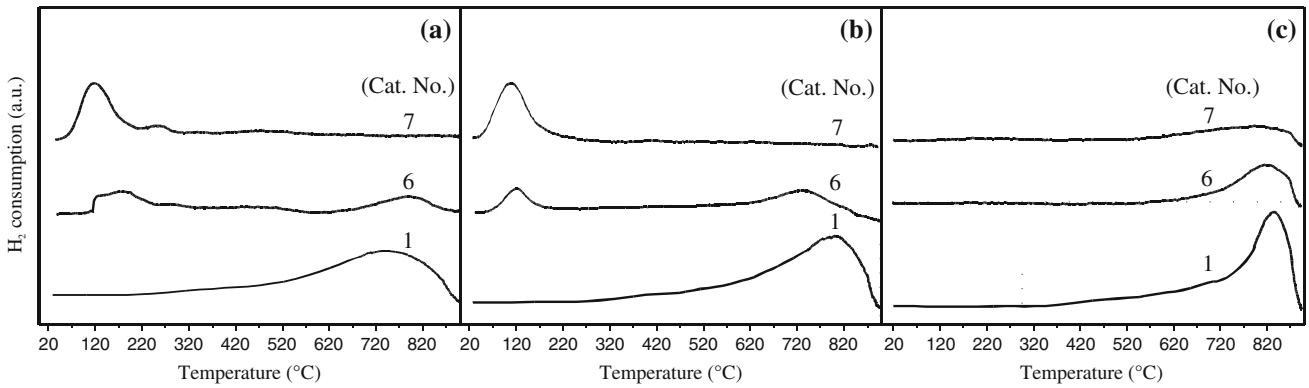


**Fig. 3** Influence of oxidation temperature on $TPR_{H2}$ of Ni–Rh/$Al_2O_3$ catalysts prepared from $Ni(NO_3)_2$ and $Rh(NO_3)_3$; **a** 500 °C, **b** 700 °C and **c** 900 °C

after calcinations of catalyst at 500 °C (see Table 1). According to Vis [15] the reduction of unsupported rhodium oxide (III) takes place in the temperature range 100–200 °C. The increase in calcination temperature from 500 to 900 °C leads to the decrease in or disappearance of easily reducible $Rh_2O_3$ in favour of atomically dispersed system of $Rh^{3+}$ ions in the surface layer of alumina forming structure $Rh^{3+}(AlO_2)_y$. However, the formation of compound-like mixed oxides of $Rh_2O_3$ and $Al_2O_3$ or rhodium aluminate with general formula $Rh(AlO_2)_y$ was not confirmed experimentally [16, 17]. In the case of 5Ni/$Al_2O_3$ catalyst the increase in the oxidation temperature results in a shift of the temperature reduction range towards higher temperatures. The comparison of $TPR_{H2}$ profiles with literature data [18–22] confirms an existence of dominant nickel (II) aluminate, which is reduced with the maximum rate at the temperature about 800 °C [22]. The reduction of bimetallic 2.5Ni–2.5Rh(n)/$Al_2O_3$ catalyst

calcined at 500 °C favours the formation of the separated individual monometallic oxide phases $Rh_2O_3$ and $NiAl_2O_4$. After calcination of this sample at 700 °C the reduction temperature of nickel aluminate is shifted towards a lower temperature. That means that Rh enhances the reducibility of $NiAl_2O_4$ species, which can increase the amount of metallic Ni during the reduction and reaction processes [23]. The calcination of the fresh bimetallic catalyst at 900 °C results in the formation of only one broad reduction peak at a high temperature ($T_{max.}$ at ~800 °C), which can correspond to a simultaneous penetration of oxide phases of Ni and Rh into alumina structure and makes the resultant system difficult to reduce.

Analogous trends in $TPR_{H2}$ behavior can be observed during the reduction of Ni–Rh/$Al_2O_3$ catalysts prepared from $Ni(NO_3)_2$ and $RhCl_3$ after calcination at 700 and 900 °C presented in Fig. 4. The characteristic features of $TPR_{H2}$ profiles for bimetallic samples after their calcination at a temperature of 700 °C refer to the changes of participation in reduction effects of rhodium and nickel oxide phases. These changes seem to be proportional to the percentage of metals in catalyst. Both the temperature ranges and magnitude of reduction effects appear to confirm a lack of significant interaction between both oxide phases of metals. The promotion effects of rhodium on the reduction of nickel oxide were not observed either, as it was in the case of bimetallic 2.5Ni–2.5Rh(n)/$Al_2O_3$ catalyst. In the case of $TPR_{H2}$ profiles for monometallic Rh/$Al_2O_3$ catalyst calcined at 700 °C one can see a peak shifting to a higher temperature in comparison with that observed for Rh(n)/$Al_2O_3$ sample (curve 7, Fig. 3b). The differences can be attributed to the presence or absence of chloride ions. Therefore, one can assume that "chlorine free" rhodium oxide $RhO_x$ ($x = 1.5$) undergoes reduction more easily than $Rh_2O_yCl_z$ ($y + 2z = 3$), which is in accordance with Hwang et al. [24]. The confirmation of such a conclusion can be $TPR_{H2}$ profile of 5Rh/$Al_2O_3$ catalyst after calcination at a temperature of 900 °C. The rhodium oxide phase of rhodium (III) chloride origin is less prone to penetrate the structure of alumina than the analogues rhodium oxide phase prepared from rhodium (III) nitrate (V). It is difficult to state that the surface of 5Rh/$Al_2O_3$ catalyst calcined at a temperature of 900 °C is free of chlorine because the surface of alumina support can stabilize $Cl^-$ ions even at the temperature as high as 800–900 °C [13].

$TPR_{H2}$ profiles similar to those of Ni–Rh/$Al_2O_3$ catalysts prepared from $Ni(NO_3)_2$ and $Rh(NO_3)_3$ calcined at 500, 700 and 900 °C were obtained for the same series of catalysts in the successive TPO-$TPR_{H2}$ cycles presented in Fig. 5. The reoxidation process after the reduction step (TPR) differs from the first oxidation (calcination) of catalyst precursor in the kind of dispersed substance submitted to oxidation. In the case of reoxidation usually the phase which undergoes oxidation is the metallic phase (crystallites), but during the first oxidation decomposition of precursor (dispersed salt of metal) takes place. Even though in both cases one can expect the dispersed oxide phase of metal, the state and nature of it can significantly differ. The less or more sintered metallic phase which was formed during the earlier reduction process ($TPR_{H2}$), is subjected to reoxidation. The first oxidation usually gives a high degree of dispersion of supported oxide phase and its interaction with the support can be stronger, which leads to the decrease in catalyst reducibility. Such an interpretation could explain the observed differences in $TPR_{H2}$ profiles of Rh(n)/$Al_2O_3$ catalyst after the first oxidation (curve 7, Fig. 3a) and reoxidation (curve 7, Fig. 5a) at the same temperature of 500 °C. The decrease in reducibility of Rh(n)/$Al_2O_3$ catalyst reoxidized at a temperature of 900 °C

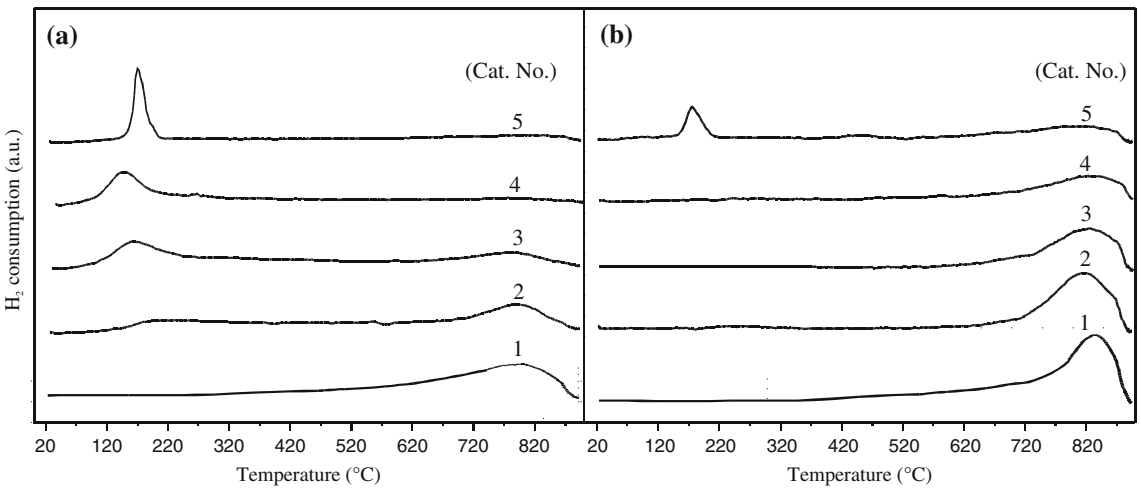


**Fig. 4** Influence of oxidation temperature on $TPR_{H2}$ of Ni–Rh/$Al_2O_3$ catalysts prepared from $Ni(NO_3)_2$ and $RhCl_3$; **a** 700 °C and **b** 900 °C

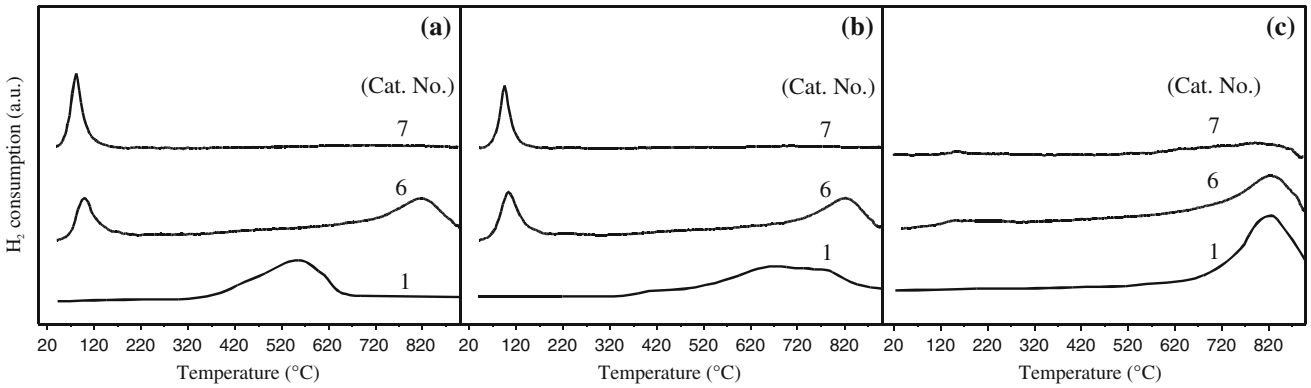


**Fig. 5** $TPR_{H2}$ profiles of Ni–Rh/$Al_2O_3$ catalysts prepared from $Ni(NO_3)_2$ and $Rh(NO_3)_3$ in successive TPR–TPO cycles: **a** after the first reoxidation at 500 °C, **b** after the second reoxidation at 700 °C and **c** after the third reoxidation at 900 °C

(curve 7, Fig. 5c) can be a result of the redispersion process of rhodium oxide phase–diffusion of $Rh^{3+}$ ions to the inside of $Al_2O_3$, which leads to the formation of a highly resistant to reduction $Rh^{3+}(AlO_2)_y$ phase. During its reduction the temperature and time can be the factors which would decide about the dispersion degree of rhodium metallic phase formed as a result of sintering. Therefore, the high temperature cycle of $H_2$–$O_2$ can be represented according to the scheme:

$$Rh/Al_2O_3 \underset{H_2,\,900^{\circ}C\,(\text{sintering})}{\overset{O_2,\,500-900^{\circ}C\,(\text{redispersion})}{\rightleftharpoons}} Rh^{3+}(AlO_2)_y \qquad (9)$$

The lack of NiO phase formation in the decomposition of bimetallic Ni–Rh/$Al_2O_3$ catalyst precursors seems to confirm a close vicinity of bimetallic oxide components and such a situation makes the alloying process more favorable during catalyst reduction in hydrogen atmosphere. Such an interpretation is confirmed by XRD measurements, carried out after the temperature programmed hydrogen assisted decomposition of Ni–Rh catalysts up to 900 °C. The same conclusion was drawn for silica supported Ni–Rh catalysts [1]. XRD patterns are presented in Fig. 6. They were obtained by subtraction of support background in order to avoid overlapping of diffraction lines of metals and support.

The broad XRD reflections signals for monometallic Rh(n)/$Al_2O_3$ catalyst (curve 7) confirm the existence of small rhodium crystallites on alumina, whereas the higher and much narrower XRD reflections for monometallic Ni/$Al_2O_3$ and Rh/$Al_2O_3$ catalysts (curve 1 and 5, respectively) indicate the growth of nickel and rhodium crystallites as a result of the sintering process taking place during the temperature programmed hydrogen assisted decomposition. The XRD reflections characteristic of bimetallic Ni–Rh/$Al_2O_3$ catalysts change their location monotonically in function of bimetal phase composition, and they are located in the range of $2\theta$ values limited by the reflections

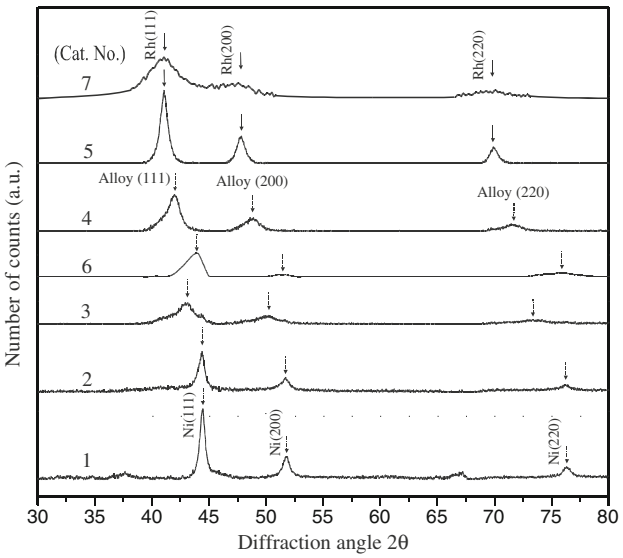


**Fig. 6** XRD patterns of Ni–Rh/$Al_2O_3$ catalysts after $TPDE_{H2}$ of their precursors up to a temperature of 900 °C

characteristic of monometallic phases Rh(111) and Ni(111) or Rh(200) and Ni(200). Similar results of XRD measurements presented in Fig. 7 were obtained for 2.5Ni–2.5Rh/$Al_2O_3$ catalyst (curve 3) after the pretreatment procedure consisting of oxidation at 500 °C in $O_2$ stream for 3 h followed by reduction at 500 °C in $H_2$ stream for 1 h.

In the case of alumina supported rhodium catalysts on the XRD patterns (curve 5 and 7) no *reflections characteristic* of metallic rhodium were observed, which can indirectly prove a high dispersion degree of rhodium on the support and it is in accordance with hydrogen chemisorption results (Table 1). The absence of nickel, rhodium or alloy phases was observed for 2.5Ni–2.5Rh(n)/$Al_2O_3$ catalyst (curve 6). XRD pattern of Ni/$Al_2O_3$ catalyst (curve 1) shows weak and broad reflections corresponding to metallic nickel and it can be concluded that the dispersion degree of nickel on the surface of alumina catalyst is lower than rhodium, which is

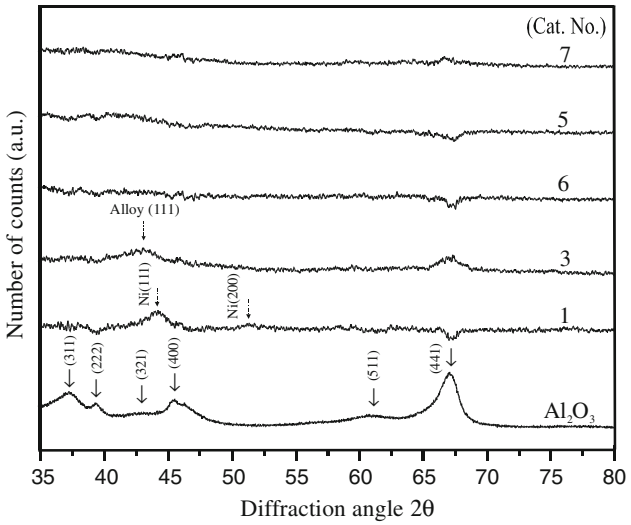


**Fig. 7** XRD patterns of Ni–Rh/$Al_2O_3$ catalysts after calcination at 500 °C/3 h followed by reduction at 600 °C/1 h

also in agreement with hydrogen chemisorption data (Table 1). The lowest XRD detection limit for metallic crystallite size was estimated as about 5 nm.

FT-IR spectra of carbon monoxide adsorption on monometallic Ni and Rh and bimetallic Ni–Rh catalysts are shown in Fig. 8.

Carbon monoxide adsorption on 5Rh/$Al_2O_3$ catalyst (curve 5) is represented by four main IR bands: two–overlapped on each other with their maxima located at 2,097 and 2,065 $cm^{-1}$, one–dominant at 2,030 $cm^{-1}$ and the last one–broad band at 1,823 $cm^{-1}$. According to the literature data IR bands at 2,097 and 2,030 $cm^{-1}$ can be assigned to rhodium *gem*-dicarbonyl species—$Rh^{+}(CO)_2$ [25] formed during reaction [26]:

$$1/xRh_x^{\circ} + OH_{(s)} + 2CO_{(g)} \leftrightarrows Rh^{+}(CO)_2 + 0.5H_2 \qquad (10)$$

where OH(s) is the isolated surface hydroxyl group on $Al_2O_3$.

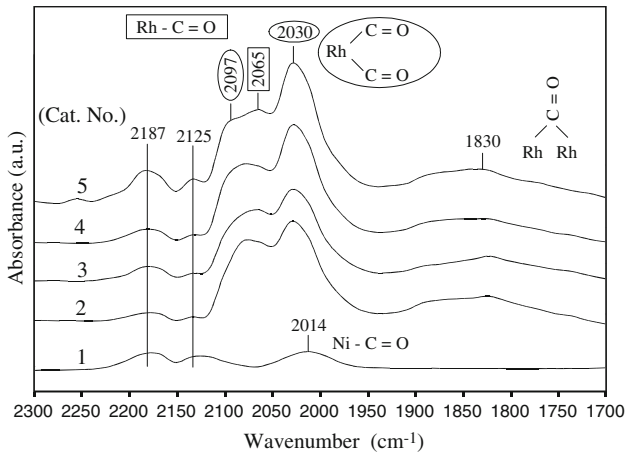


**Fig. 8** FT-IR spectra of CO adsorption (1 atm, 25 °C) on mono- and bimetallic Ni–Rh/$Al_2O_3$ catalysts prepared from $Ni(NO_3)_2$ and $RhCl_3$

It is known that *gem*-dicarbonyls are formed on active centres which are isolated rhodium atoms (rhodium in an atomically dispersed state) [27, 28]. The same literature data reveal that their formation is more facile on highly dispersed rhodium supported on alumina [27, 28] than on silica [26]. It also seems to be confirmed by a significantly higher dispersion degree of rhodium supported on alumina than on silica [1]. Van't Bilk et al. [29] showed on the basis of EXAFS method that CO adsorption on small Rh crystallites causes the disruption of the Rh–Rh distances, i.e., the production of isolated sites capable of forming the *gem*-dicarbonyl species.

The appearance of weak IR band at 2,065 $cm^{-1}$ and low intensity band at 1,830 $cm^{-1}$ can be attributed to linear and bridged forms of CO adsorption on $RhAl_2O_3$, respectively [30]. FTIR spectrum of monometallic nickel catalyst supported on alumina (curve 1) is characterized by one IR band placed at the same wavenumber as for Ni/$SiO_2$ catalyst [1]. This band (at 2,014 $cm^{-1}$) is characteristic of the linear form of CO adsorbed on the surface of metallic nickel [31]. Infrared spectra of CO adsorbed on bimetallic Ni–Rh/$Al_2O_3$ catalysts (curves 2–4) are very similar to those characteristic of monometallic Rh/$Al_2O_3$ catalyst, which can result from the lower dispersion of Ni, incomplete reduction of the NiO and to IR bands overlapping. This experimental assignment does not seem to confirm the enrichment of nickel on the surface of bimetallic alloy, in contrast to earlier studies of Ni–Rh/$SiO_2$ systems [1].

Average values of $Ni^{+}/Rh^{+}$ ions intensity ratio calculated on the basis of ToF-SIMS spectra recorded for 2.5Ni–2.5Rh/$Al_2O_3$ catalyst prepared from $RhCl_3$ precursor, after its treatment in $O_2$ stream at 500 °C/3 h and next in $H_2$ flow at 600 °C/1 h were shown in Table 2. It can be observed that average value of $Ni^{+}/Rh^{+}$ ions intensity ratio increased after reduction of calcined 2.5Ni–2.5Rh/$Al_2O_3$ catalyst. On the other hand the results of the measurements of the samples after removal of some part of surface layers do not reveal any significant differences in the value of $Ni^{+}/Rh^{+}$ intensity ratio. It confirms the enrichment of nickel on the surface of bimetallic Ni–Rh alloy after reduction of the catalyst.

### 3.2 Catalytic Test and Coke Deposition

The influence of temperature on catalytic activity of mono Ni, Rh and bimetallic Ni–Rh catalysts, obtained from $RhCl_3$ and $Rh(NO_3)_3$ precursors, in $CO_2$ reforming of methane is presented in Figs. 9 and 10, respectively. This reaction starts at about 300 °C and its rate increases monotonically up to about 850 °C.

The curves representing both monometallic Rh and bimetallic Ni–Rh/$Al_2O_3$ catalysts in Fig. 9 do not differ very much and all tested samples can be regarded as very active catalysts. The monometallic nickel catalyst was the

**Table 2** Average value of $Ni^+/Rh^+$ ions intensity ratio calculated on the basis of ToF-SIMS spectra recorded for 2.5Ni–2.5Rh/$Al_2O_3$ catalyst prepared from $RhCl_3$ precursor

| No. | Catalyst | Thermal treatment | Average value of $Ni^+/Rh^+$ ions intensity ratio | |
|---|---|---|---|---|
| | | | "As prepared" catalyst surface | Catalyst surface after sputtering |
| 3 | 2.5Ni–2.5Rh | $O_2$, 500 °C, 3 h | 0.9 | 1.8 |
| | | $O_2$, 500 °C, 3 h → $H_2$, 600 °C, 1 h | 2.2 | 1.6 |

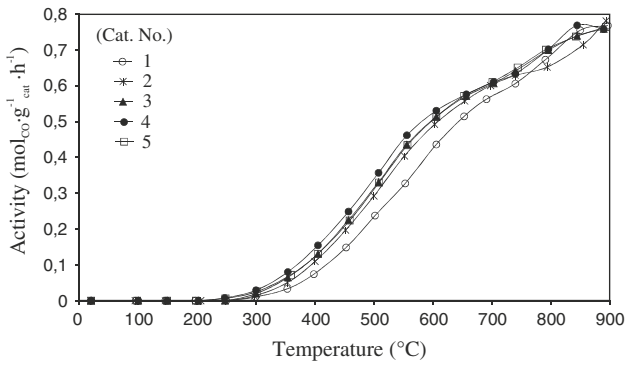


**Fig. 9** The influence of temperature on catalytic activity of Ni–Rh/$Al_2O_3$ catalysts prepared from $Ni(NO_3)_2$ and $RhCl_3$ in $CH_4/CO_2$ reforming ($CH_4/CO_2$ = 1:1, W/F = 3.33 × $10^{-5}$ g h $cm^{-3}$)

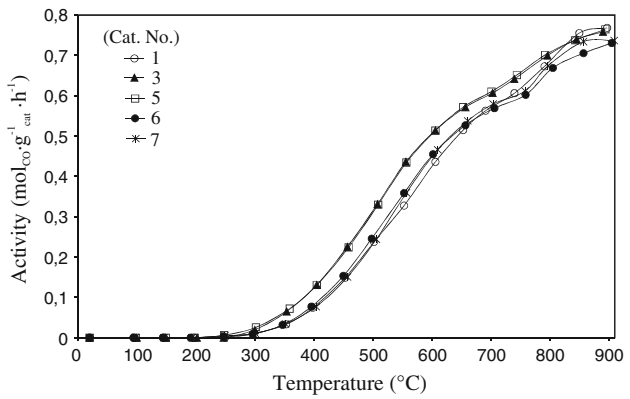


**Fig. 10** The influence of temperature on catalytic activity of Ni–Rh/$Al_2O_3$ catalysts prepared from $Ni(NO_3)_2$ and $Rh(NO_3)_3$ in $CH_4/CO_2$ reforming of methane ($CH_4/CO_2$ = 1:1, W/F = 3.33 × $10^{-5}$ g h $cm^{-3}$)

least active in the whole temperature range. The monometallic Rh(n) and bimetallic Ni–Rh(n)/$Al_2O_3$ catalysts show similar activity (Fig. 10). Catalysts obtained from $RhCl_3$—Rh/$Al_2O_3$ and 2.5Ni–2.5Rh/$Al_2O_3$ proved to be the most active.

More detailed information referring to the conversion data at 700 °C is presented in Table 3 as: $CH_4$ and $CO_2$ conversion, yields of CO and $H_2$ and the activity calculated as mol CO $g^{-1}$ $h^{-1}$ and turnover frequency (TOF). The presented data show close resemblance of catalytic behaviour for monometallic and bimetallic nickel and rhodium catalysts. The $CO_2$ conversion (79–89%) was practically always higher than $CH_4$ conversion (72–87%) and the difference is ascribed to the occurrence of the reverse water-shift reaction simultaneously with the reforming reaction [32]. The decreasing tendency of TOF values from about 8 to about 1 with the increase in rhodium loading is attributed to a considerably higher rhodium dispersion in comparison with the nickel one (Table 1).

Table 3 also presents the initial catalyst activity, its loss after 24 h on stream at 700 °C and a total amount of coke deposited on the catalyst surface during this time. The losses of catalyst activity were in the range 0–9% of their initial values. There is no simple correlation between the coke deposition taking place in the course of reaction and the loss of catalyst activity. However, loss of catalyst stability does not have to be caused by coke deposition of catalyst, as it is observed in the case of monometallic 5Rh(n)/$Al_2O_3$ catalyst (Table 3). It is known that except for the coke deposition at least two factors can contribute to deactivation of catalysts like sintering and poisoning by the substances coming from the support [33, 34]. Also the tendency to coke formation does not have to reflect the loss of activity, as it is for bimetallic 2.5Ni–2.5Rh(n)/$Al_2O_3$ catalyst (Table 3). Among all studied catalysts monometallic rhodium catalyst prepared from rhodium (III) chloride and bimetallic nickel rich catalysts are distinguished by both the highest catalytic stability after 24 h work and the lowest degree of coke deposition. In the case of rhodium supported on alumina, which is considered as storage of hydroxyl group because of high concentration of acid and basic centres on its surface [35], the $OH^-$ groups play a key role in obtaining high catalytic stability of Rh/$Al_2O_3$ catalyst as an effect of decreasing the rate of coke deposition on metal. Weaker basic support surface sites can be anticipated in the case of chloride ions originating from reaction 8. The highest loss of stability (9%) and the tendency to coke formation (3%) was found for monometallic Ni/$Al_2O_3$ catalyst. The obtained results of $CO_2$, $CH_4$ conversion, stability test and deposited coke for monometallic Ni and Rh alumina—supported catalysts are similar to the published data [23]. The Ni–Rh/$Al_2O_3$ catalysts appeared more stable and resistant to coke deposition in comparison with the earlier reported Ni–Rh catalysts supported on $SiO_2$ [1]. Acidic character of $CO_2$ molecule would rather favor more basic surface of alumina than silica. Thus, the

**Table 3** Characterization of mono- and bimetallic Ni–Rh/$Al_2O_3$ catalysts

| No. | Catalyst | $CH_4$[a] conversion (%) | $CO_2$[a] conversion (%) | Yield[a] of CO (%) | Yield[a] of $H_2$ (%) | $TOF_{CO}$[a] ($s^{-1}$) | Activity[a] ($mol_{CO}\ g_{cat}^{-1}\ h^{-1}$) | Loss of activity (%)[b] | TOC[c] (wt.%) |
|---|---|---|---|---|---|---|---|---|---|
| 1 | 5Ni | 72 | 79 | 73 | 58 | 7.9 | 0.562 | 9.1 | 3.2 |
| 2 | 3.75Ni–1.25Rh | 80 | 82 | 77 | 61 | 6.2 | 0.601 | 0.6 | 0.6 |
| 3 | 2.5Ni–2.5Rh | 84 | 86 | 80 | 63 | 6.5 | 0.608 | n.o. | 0.3 |
| 4 | 1.25Ni–3.75Rh | 87 | 88 | 81 | 64 | 1.8 | 0.612 | 2.8 | 0.8 |
| 5 | 5Rh | 82 | 87 | 80 | 63 | 0.9 | 0.612 | n.o. | 0.4 |
| 6 | 2.5Ni–2.5Rh (n) | 84 | 84 | 78 | 62 | 1.5 | 0.569 | n.o. | 1.0 |
| 7 | 5Rh (n) | 83 | 86 | 79 | 63 | 0.8 | 0.580 | 2.7 | 0.6 |

(n) indicates precursor of Rh–$Rh(NO_3)_3$

[a] Measured at 700 °C

[b] Measured after 24 h on stream, reaction temperature 700 °C; $W/F = 3.33 \times 10^{-5}$ g h $mL^{-1}$

[c] Total amount of carbon

n.o. = not observed

expected higher $CO_2$ coverage of alumina support would not only promote catalytic activity in the interphase support-metal region of dry reforming of methane but could also prevent from the excessive formation of catalyst deactivated carbon in an accompanying side reaction $CO_2 + C \rightarrow 2CO$. The second accompanying reaction—reverse water gas shift $CO_2 + H_2 \rightarrow CO + H_2O$ leads to higher yield of CO and lower yield of $H_2$.

## 4 Conclusions

The surface characteristics of $Al_2O_3$-supported mono-Ni, Rh and bimetallic Ni–Rh catalysts and their catalytic performance for carbon dioxide reforming of methane were studied. The following main conclusions can be pointed out: (i) the $Al_2O_3$ supported monometallic Ni, Rh and bimetallic Ni–Rh catalysts are comparably good catalysts for carbon dioxide reforming of methane; (ii) effective process of Ni–Rh alloy formation takes place in the case of $Al_2O_3$ supported bimetallic Ni–Rh catalysts; (iii) the precursor of rhodium ($Rh(NO_3)_3$ or $RhCl_3$) influences the promoting effect of this metal on the reducibility of nickel oxide; (iv) segregation of metals can lead to the formation of Ni-rich surface alloy.

**Acknowledgments** This work was partially supported by Grant No. PBZ/KBN/116/T09/2004 of the State Committee for Scientific Research. The authors are indebted to Prof. R. Fiedorow from the Adam Mickiewicz University of Poznan (UAM) for carrying out hydrogen chemisorption measurements.

## References

1. Jóźwiak WK, Nowosielska M, Rynkowski JM (2005) Appl Catal A 280:233
2. Wang HY, Ruckenstein E (2000) Appl Catal A 204:143
3. Nandini A, Pant KK, Dhingra SC (2005) Appl Catal A 290:166
4. Hou Z, Yokota O, Tanaka T, Yashima T (2003) Appl Catal A 253:381
5. Juan-Juan J, Román-Martínez MC, Illán-Gómez MJ (2004) Appl Catal A 264:169
6. Riva R, Miessner H, Vitali R, Del Piero G (2000) Appl Catal A 196:111
7. Williams FL, Nason D (1974) Surf Sci 45:377
8. Hultgren R, Orr RL, Anderson PD, Kelly K (1963) Selected values of thermodynamic properties of metals and alloys. Wiley, New York
9. Leclercq G, Pietrzyk S, Gengembre L, Leclercq L (1986) Appl Catal 27:299
10. Irusta S, Cornaglia LM, Lombardo EA (2002) J Catal 210:7
11. Irusta S, Cornaglia LM, Lombardo EA (2002) J Catal 210:263
12. Silva LMS, Órfão JJM, Figueiredo JL (2001) Appl Catal A 209:145
13. Maniecki TP (2002) Doctor's Thesis, Institute of General and Ecological Chemistry, Technical University of Łódź
14. Hou Z, Yashima T (2003) Catal Lett 89:193
15. Vis JK Doctor's Thesis, Eindhoven, Holandia
16. Burch R, Loader PK, Cruise NA (1996) Appl Catal A 147:375
17. Wang R, Xu H, Liu X, Ge Q, Li W (2006) Appl Catal A 305:204
18. Rynkowski JM, Paryjczak T, Lenik M (1995) Appl Catal A 126:257
19. Lee J-H, Lee E-G, Joo O-S, Jung K-D (2004) Appl Catal A 269:1
20. Rynkowski JM, Paryjczak T, Lenik M (1993) Appl Catal A 106:73
21. Li B, Watanabe R, Maruyama K, Nurunnabi M, Kunimori K, Tomishige K (2005) Appl Catal A 290:36
22. Rzeźnicka I, Góralski J, Paryjczak T (2001) Chem Environ Res 10:47
23. Hou Z, Chen P, Fang H, Zheng X, Yashima T (2006) Int J Hydrogen Energy 31:555
24. Hwang Ch, Yeh Ch, Zhu Q (1999) Catal Today 51:93
25. Wang HP, Yates JT Jr (1984) J Catal 89:79
26. Chuang SSC, Tan Ch (1997) Catal Today 35:369
27. Solymosi F, Pásztor M (1986) J Phys Chem 90:5312
28. Yates JT, Duncan TM, Vanghan RW (1979) J Phys Chem 71:3908
29. van't Bilk HFA, Dvon Zon JBA, Hulzinga T, Vis JC, Koningsberger DC, Prins R (1983) J Phys Chem 87:2264
30. Bulushev D, Froment GF (1999) J Mol Catal A Chem 139:63

31. Agnelli M, Swaan HM, Marquez-Alvarez C, Martin GA, Mirodatos C (1998) J Catal 175:117
32. de Souza MMVM, Clavé L, Dubois V, Perez CAC, Schmal M (2004) Appl. Catal. A 272:133
33. Lewicki A, Paryjczak T, Jóźwiak WK, Rynkowski JM (2002) Wiad Chem 56:279
34. Zhang ZL, Tsipouriari VA, Efstathiou AM, Verykios XE (1996) J Catal 158:51
35. Schuurman Y, Marquez-Alvarez C, Kroll VCH, Mirodatos C (1998) Catal Today 46:185